Final Draft

of the original manuscript:

Schmoelzer, T.; Liss, K.-D.; Kirchlechner, C.; Mayer, S.; Stark, A.;
Peel, M.; Clemens, H.:

An in-situ high-energy X-ray diffraction study on the hot-deformation behavior of a Beta-phase containing TiAl alloy

An in-situ high-energy X-ray diffraction study on the hot-deformation behavior of a β-phase containing TiAl alloy

T. Schmoelzer [a], K.-D. Liss [b], C. Kirchlechner [c], S. Mayer [a], A. Stark [d], M. Peel [e], H. Clemens [a]

[a] Department of Physical Metallurgy and Materials Testing, Montanuniversität Leoben, 8700 Leoben, Austria.

[b] The Bragg Institute, ANSTO, Lucas Heights, New South Wales 2232, Australia.

[c] Department Material Physics, Montanuniversität Leoben, 8700 Leoben, Austria.

[d] Institute of Materials Research, Helmholtz-Zentrum Geesthacht, 21502 Geesthacht, Germany.

[e] European Synchrotron Radiation Facility, BP 220, 38043 Grenoble, France.

Abstract

In engineering materials, microstructural evolution during hot-working critically determines the properties of the finished part. Intermetallic TiAl alloys are no exemption from this common observation and numerous attempts have been made to improve their performance by subjecting them to harmonized hot-working steps. In the current work a novel in-situ diffraction technique along with conventional microscopic methods were employed to characterize the behavior of the individual phases at two different deformation temperatures. A so-called TNM™ alloy with a nominal composition of Ti-43.5 Al-4 Nb-1 Mo-0.1 B (in at%), which exhibits an adjustable fraction of disordered β-phase at elevated temperatures, was deformed isothermally at 1220 °C and 1300 °C. At 1220 °C three phases (α,β,γ) are existent, whereas at 1300 °C two phases (α,β) are present in thermodynamic equilibrium. It was possible to observe in-situ the individual behavior of the involved phases during

deformation and the phenomena which accommodate the defects generated by hot-working. Results of post mortem microscopic investigations were used to confirm the findings. Especially the results of the in-situ experiments give unique insights into the hot-deformation behavior of multi-phase TiAl alloys, which can be used for specific process optimization and for further alloy development.

1 Introduction

Intermetallic γ-TiAl alloys exhibit high strength at elevated temperatures while having low density [1–5]. These properties make them an attractive material for the application in turbine blades of aero-engines as well as in turbocharger turbine wheels for reciprocating engines [6–9]. Due to the continuous strive of manufacturers to improve engine efficiencies, the demands on the performance of components are ever increasing. A transition in the production route, from casting towards implementation of a hot-working step, combined with subsequent heat-treatments is expected to enable a more thorough control of the microstructure and thus improve the mechanical properties of the finished part [10–12].

Alloys of the so-called TNM™ family can be forged using an isothermal or a near-conventional process [7,13,14]. This type of alloy is particularly well suited for forging and rolling due to the presence< of the ductile, disordered body-centered cubic (bcc) β-phase at hot-deformation temperatures [10,13,15]. While it is well established that the β-phase promotes the hot-deformation behavior [16–18], it is not clear which microstructural mechanisms act during forging. A number of papers were published concerning the hot-deformation of γ-TiAl alloys. Most of them report on compression experiments performed at different temperatures and strain rates where the specimens were subjected to subsequent microstructural investigations [19–24]. Post-mortem investigations of the processes occurring during forging are complicated

by the fact that multiple phase transformations and ordering reactions may occur upon cooling to room-temperature. Information on phase equilibria and transformation temperatures in the Ti-Al system can be found in [25]. Recent studies on the pseudo-binary phase diagram of TNM™ alloys are provided in [26–28]. Frequently, also the shape of the flow-curve is used for obtaining information on microstructural processes [20,22–24]. In a multiphase material, the flow behavior is determined by the deformation response of each individual phase and the interaction between these phases. Thus, information obtained from the flow-curve predominantly describes the behavior of the majority phase. Additionally, it is notable that most experiments on TiAl alloys were conducted within the $(\alpha_2+\gamma)$ $(\alpha+\gamma)$ or $(\alpha+\beta_o+\gamma)$ phase field regions. Consequently, little information concerning deformation at very high temperatures, i.e. in the $(\alpha+\beta)$ phase field region is available.

In this study, an attempt was made to observe the behavior of an engineering β-containing TiAl alloy in-situ during hot-deformation. To this end, a high-energy X-ray diffraction (HEXRD) method developed by Liss et al was utilized [29–31]. The findings obtained by the in-situ method were confirmed by the results of post-mortem microstructural investigations. Performing in-situ experiments at two different temperatures (in the $(\alpha+\beta)$ and the $(\alpha+\beta+\gamma)$ phase field regions) allows comparison of the deformation behavior dependent on the phases present. The obtained results ultimately contributed to determining suitable process parameters for industrial forming operations [12,13].

Materials and Methods

The alloy investigated had a nominal chemical composition of Ti-43.5 Al-4 Nb-1 Mo-0.1 B (in at%) and was supplied by GfE Metalle und Materialien GmbH, Nuremberg, Germany. Ingots with a diameter of 55 mm were produced by means of

centrifugal casting. To close residual porosity, the ingot was subsequently hot-isostatically pressed (HIPed) at a temperature of 1200 °C and a pressure of 200 MPa for 4 h. The three main phases are the α_2-Ti_3Al ($D0_{19}$ structure), the β_o-Ti phase (B2 structure) as well as their disordered polymorphs (α: A3 structure, β: A2) and the γ-TiAl phase ($L1_0$). The β/β_o-phase fraction has a minimum at 1285 °C which is also the transition temperature between the ($\alpha+\beta$) and ($\alpha+\beta+\gamma$) phase field region. A pseudo-binary section of the phase diagram calculated with a commercial TiAl data base [32] is presented in Figure *phase* a. Additionally, the alloy composition and the deformation temperatures are indicated. Together with the course of phase fractions over temperature shown in Figure *phase* b, these data were acquired during a previous study [27]. For further details, especially on the difference between calculated and experimentally established phase diagrams, the reader is referred to [26–28]. At 1300 °C, i.e. in the ($\alpha+\beta$) phase field region, the volume fractions of α and β are approximately 93 vol% and 7 vol% whereas at 1220 °C, volume fractions of α, β, and γ were determined to 46 vol%, 13 vol%, and 93 vol% respectively. In Figure *phase*b, the $\beta_o \leftrightarrow \beta$ and $\alpha_2 \leftrightarrow \alpha$ order/disorder temperatures obtained from neutron diffraction experiments are indicated [33]. As the phenomena occurring during deformation are discussed, it should be born in mind that the experiments were conducted at very high homologous temperatures. A deformation temperature of 1300 °C corresponds to approximately $0.87 \times T_m$ whereas 1220 °C are equivalent to $0.82 \times T_m$.
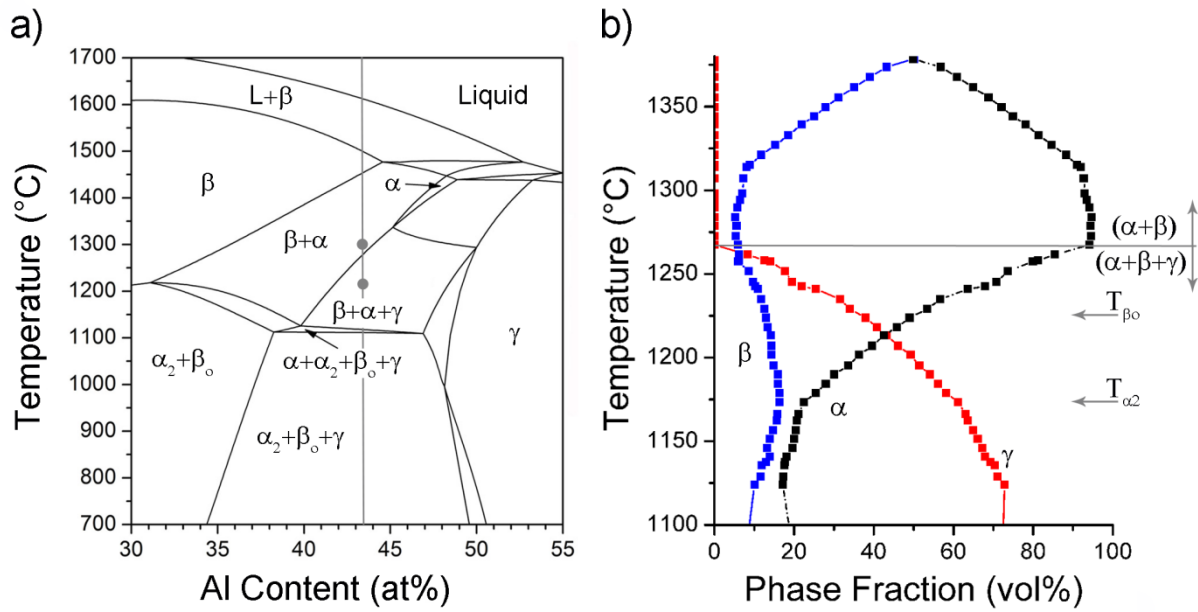
Figure *phase*: (a) calculated binary section of the quaternary phase diagram [26] and (b) experimentally determined course of phase fractions over temperature of the investigated alloy [27]. In (a), the alloy composition is indicated by a vertical line, the two deformation temperatures are marked by filled circles. Order/disorder transition temperatures of α_2/α and β_o/β are indicated by $T_{\alpha2}$ and $T_{\beta o}$, respectively in (b) [33].

The experimental setup for investigating dynamic microstructural processes with high-energy X-rays is very similar to that of a conventional powder diffraction experiment at a synchrotron source. In the illuminated specimen volume, a limited number of grains should be contained to be able to distinguish single diffraction spots on the Debye-Scherrer rings. Yet a sufficiently high number of grains have to be observed to allow drawing conclusions about the prevailing microstructure. A suitable condition was achieved by using a monochromatic beam with a mean energy of 86.94 keV and a cross-section of 0.1 × 0.1 mm^2 as well as cylindrical specimens with a diameter of 4 mm and a length of 8 mm. Diffraction patterns were recorded at a frame rate of about 2 Hz by a Pixium 4700 flat panel detector [34] (Thales Group,

5

Neuilly-sur-Seine, France) which was placed at a distance of 1233.8 mm from the specimen position. The sample-detector distance was determined by means of triangulation and the mean energy of the beam calibrated by employing a CeO_2 standard.

An electro-thermomechanical tester (ETMT) (Instron, Norwood, MA, USA) was utilized for heating and deforming the samples. With this device, heating was achieved resistively with a maximum current of 450 A at 8 V while loads of up to 3 kN can be imposed on the specimen. The temperature was measured with a type S thermocouple formed to a melt bead which was spot-welded directly onto the specimen surface. Inserting Ta and graphite foil between the specimen and the anvils provided a diffusion barrier and decreased friction forces at the interface. Since the ETMT has a moving and a stationary anvil, the motorized table that carried the ETMT was controlled in such a way that the beam illuminated the same specimen volume throughout the entire experiment.

The specimens were heated to the intended temperatures (1220 °C and 1300 °C) at a rate of 10 °C/s and held at this temperature for 30 s. Then, compression started with a constant anvil speed of 0.021 mm/s which translates to a mean strain rate of $3.7 \cdot 10^{-3}$ s^{-1}. During the experiment performed at 1300 °C, deformation was discontinued for 20 s to investigate the corresponding materials response. Although the experiment was set up for isothermal deformation the temperature started to decrease at high strains. This was caused by the increase in specimen diameter during compression which lead to a decrease in electrical resistance and, correspondingly, the heating power. After a total strain of $\varphi \sim -0.9$, the experiments were terminated.

As dynamic processes are occurring in the microstructure of the specimen, both during heating and deformation, the morphology of the reflection spots in the

diffraction pattern changes. Broadening of a spot can be caused by the introduction of defects into the lattice. Sub-grain formation may be identified by the dissociation of one diffraction spot into a set of individual peaks within a narrow angular range [35]. A crystallite of small size is represented by a sphere of finite radius rather than a point in reciprocal space and, hence, produces also a broader diffraction spot [36]. Additionally, if the diffraction patterns are recorded continuously, grain rotation can be detected during plastic deformation [37]. It has, however, to be born in mind that a grain which satisfies the Bragg-condition only continues to do so if its rotation axis is parallel to the incident beam. Texture evolution during hot-working becomes evident in the intensity distribution over the azimuthal angle and the different Debye-Scherrer rings [38]. In a kinematic approximation, the intensity of the individual diffraction spots is proportional to the volume of the corresponding crystallites [36]. More details on the employed diffraction method can be found in [29–31,39,40]. To illustrate the development of reflections with time, the intensity on one Debye-Scherrer ring is plotted in greyscale as a function of azimuthal angle and time. In these azimuthal angle time plots (called AT-plots henceforth) a stationary reflection spot produces a continuous line. If the line is tilted, the spot (and hence, the grain) rotates about the beam axis. Such lines are called timelines in the following. More details on the generation and interpretation of an AT-plot can be found in [30,31].

After completion of the experiments, microstructural investigations were performed on the deformed specimens. For obtaining the micrographs, a Zeiss EVO 50 scanning electron microscope (SEM) was used at an acceleration voltage of 20 kV in back scattered electron (BSE) imaging mode. Electron backscatter diffraction (EBSD) images were obtained on a LEO field emission gun SEM (Zeiss 1225) equipped with an EDAX EBSD system. An acceleration voltage of 30 kV and a 120 µm aperture were used for image acquisition.

3 Results

After casting and HIPing, the material exhibits a microstructure as shown in Figure *cast*. In this condition, colonies consisting of coarse α_2 and γ lamellae as well as globular γ-grains are present. The lamellar colonies have a broad size distribution with the largest ones reaching lengths of up to 200 µm, whereas the maximum diameter of the globular γ-grains is about 20 µm. A substantial amount of β_o-phase is observed which encompasses the lamellar colonies. Additionally, small β_o precipitates can be found within the α$_2$-laths of the lamellar colonies. It should be noted that the relatively fine-grained cast microstructure shown in Figure *cast* is achieved by the addition of boron. A good chemical homogeneity is attained by solidification via the β-phase [10].
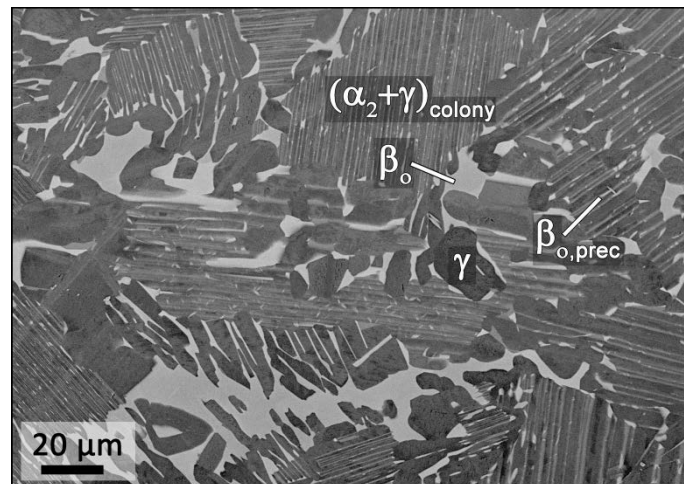

Figure *cast*: Microstructure of the cast and HIPed starting material. Three phases are present of which β_o images brightest, α_2 appears in an intermediate shade of grey and γ is the darkest phase. The image was obtained by means of SEM in BSE contrast.

Microstructural images obtained from the specimens deformed during the in-situ HEXRD experiments at 1300 °C and 1220 °C are depicted in Figure *def*. Due to the high cooling rate, the two-phase (α+β) microstructure present at a deformation temperature of 1300 °C was preserved in *def* a. Upon cooling, only the α→α_2 and β→β_o ordering reactions took place. The β_o-grains have attained a form that is more elongated perpendicular to the compression direction than the α-grains. Additionally, the complex shapes of the β_o-grains should be noted. Figure *def*b shows a microstructural image of the specimen deformed at 1220 °C in the (α+β+γ) phase field. Consequently all three phases are observed in the micrograph. The γ-phase is present in the form of globular grains and coarse lamellae within colonies, some of which have buckled during deformation. It is worth mentioning that no γ-lamellae oriented parallel to the compression direction were observed. Lamellae that buckled during deformation appear to have been the ones that were initially parallel to the loading axis (Figure *def*b inset). Compared to the starting microstructure (Figure *cast*), grain refinement is more pronounced in the specimen deformed at 1220 °C (Figure *def*b) than in the one deformed at 1300 °C (Figure *def*a).
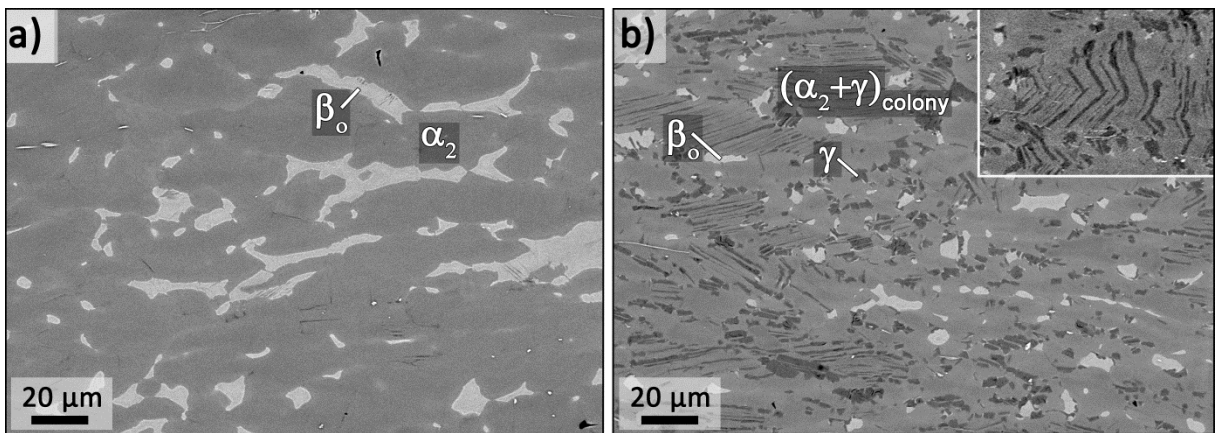

Figure *def*: Microstructures after deformation at 1300 °C (a) and 1220 °C (b). In (a) only α_2 and β_o-phase are present while in (b) also γ-phase is evident. Labels in

the micrographs indicate the phases present during hot-deformation. The inset in (b) shows lamellae that buckled during compression. In both images the compression direction is vertical and the scale of the inset is identical to the main image (b).

AT-plots of the deformation experiments performed at 1300 °C and 1220 °C as well as the parameters temperature, true stress, and true strain are presented in Figure *AT*a-f. For two representative reflections, $\alpha\,022$ (Figure *AT*a) and $\beta\,002$ (Figure *AT*b), the development of diffraction patterns over time is given only for azimuthal angles between 0° and 180° to avoid the use of overly large images.

Figures *AT*c and f show the development of temperature, true stress and true strain as a function of time. Both experiments were performed isothermally, yet at some point the specimen temperature started to decrease. At the same time the flow-stress increased which is a manifestation of the temperature dependence of the flow-stress in TiAl alloys [20,24]. Deformation was intentionally discontinued for 20 s during the experiment performed at 1300 °C to be able to observe static annealing phenomena.

During continuous heating to 1300 °C, at about 1280 °C, a sudden change in the intensity of α reflections (Figure *AT*a) occurs while some of the β spots intensify and new ones are appearing (Figure *AT*b). While holding at 1300 °C, the α-phase reflections are static, whereas the β spots show some degree of fluctuation. As deformation starts, α-phase timelines tilt, some bifurcate and all of them broaden. In the AT plots of the β-phase, dot-clouds are formed almost instantaneously. After 217 s, deformation was discontinued and the static behavior of the material can be observed.
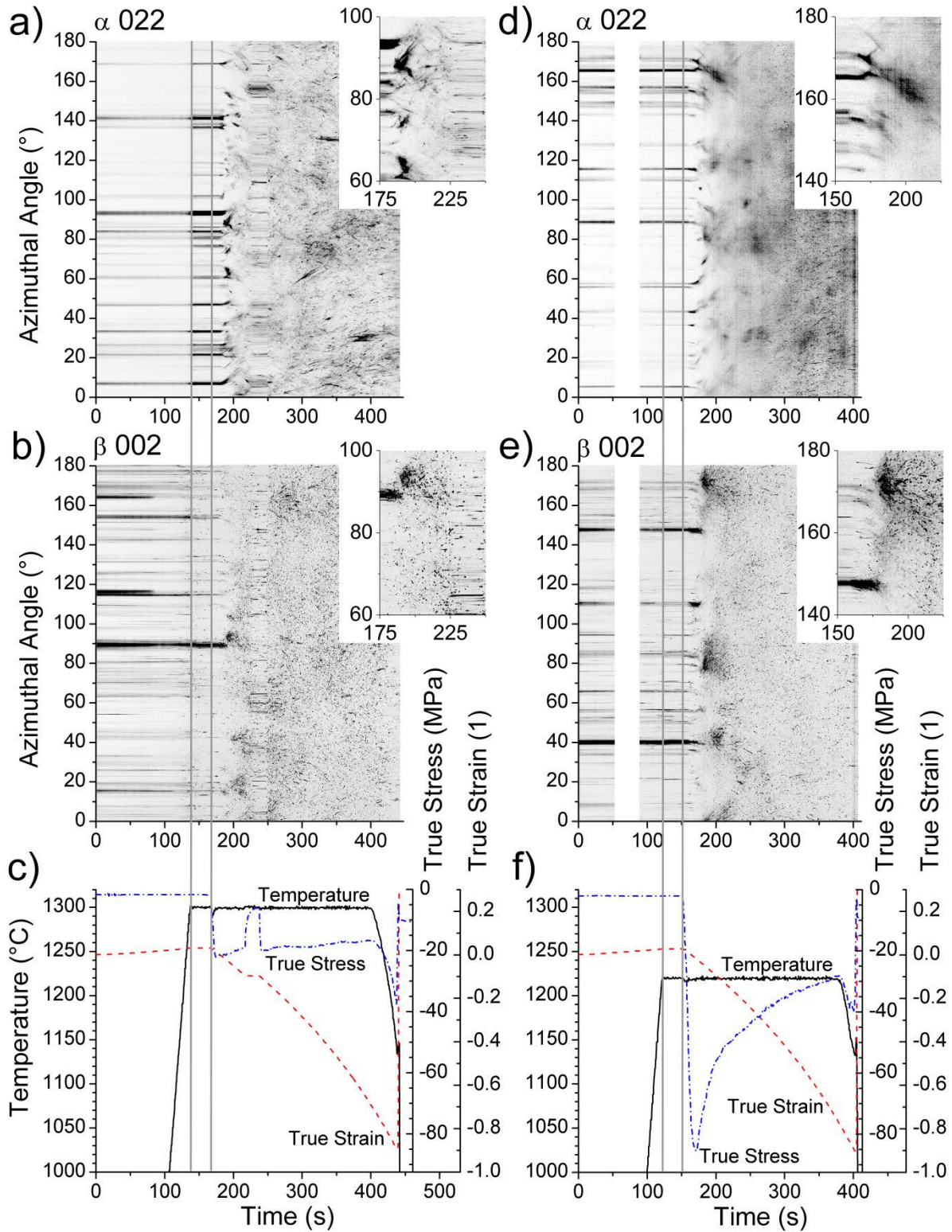
Figure *AT*: AT plots of specimens deformed at 1300 °C (left column) and at 1220 °C (right column). Both, α 022 (a,d) and β 002 (b,e) reflections are imaged as well as temperature, true stress and true strain (c,f) throughout the hot compression experiment. During heating, the temperature increases linearly from RT to

deformation temperature. Temperature values below 1000 °C are omitted to improve readability. The vertical lines mark reaching of the deformation temperature and the onset of loading while the insets provide a magnified view of pattern development at the beginning of deformation.

For both phases the number of timelines observed while deformation was stopped is greater than that before the onset of deformation. This indicates that grain refinement has occurred. Once more, the α-phase grains produce timelines in which only a few intensity fluctuations are present. The β-phase, on the other hand, exhibits strongly fluctuating intensity. As deformation continues at 1300 °C, the α-phase timelines tilt again, whereas those of the β-phase disintegrate into dots. Upon further deformation only dots are observed in the AT-plot of the β-phase (Figure *AT*b). The plot of the α-phase, on the other hand, reveals a few timelines of high intensity that are inclined with respect to the time axis (Figure°*AT*a). Generally, timelines of the α-phase are longer and sharper than those of the β-phase.

The AT-plots of α and β-phase of the experiment performed at 1220 °C are shown in Figures *AT*d and *AT*e. No images were acquired between 54 s and 89 s due to the fact that the detector routine was interrupted and had to be restarted. Since no fluctuations occur in the α or β-phase after the period during which no images were recorded, it can be assumed that no important microstructural developments were missed during heating. Again, during the holding time only the β reflections fluctuate in intensity (Figure *AT*d, e). As deformation commences, the α-phase timelines instantly broaden and are increasingly blurred as deformation increases. Starting at 270 s, comparably sharp reflection dots are appearing in the AT-plot of the α-phase. The AT-plot of the β-phase reveals the splitting of timelines

into dot-clouds when deformation starts and only a few short, comparably sharp timelines are observed until the final deformation is attained (Figure *AT*e).

In the investigated alloy, also γ-phase is present at 1220 and the AT-plot of its 020 reflection is presented in Figure *ATg*a. During heating, only gradual changes in intensity are observed. Similar to all other phases the majority of γ timelines broaden as deformation starts. Some, however, remain sharp for a long period of time (see inset in Figure *ATg*a). With increasing strain sharp dots appear which are of low intensity. Single timelines are increasingly difficult to see as deformation progresses.
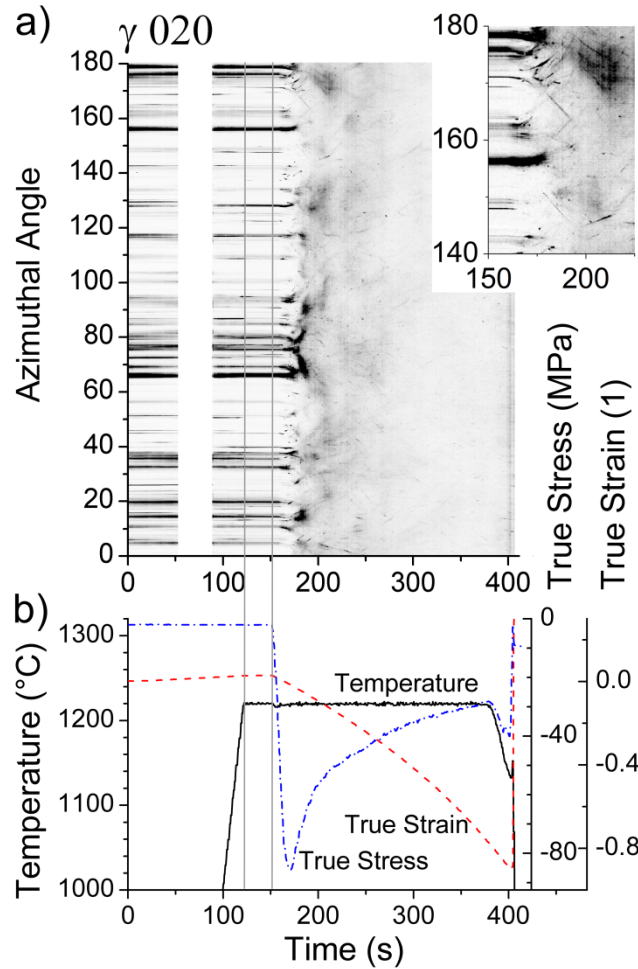

Figure *ATg*: (a) AT-plot of the γ 020 reflection of the specimen deformed at 1220 °C and (b) the corresponding deformation parameters. In the inset, a section of the AT-plot is magnified. The axes of the inset correspond to the axes of the AT-plot.

Temperature values below 1000 °C are omitted to improve readability. Vertical lines mark reaching of the deformation temperature and the onset of loading.

During the experiment, the load imposed on the specimen and the anvil position were recorded. Together with the starting geometry of the specimens, these data allow calculating the true stress and true strain under the assumptions that the specimens retain a cylindrical shape and their volumes remain constant. Stress-strain curves that were attained in this fashion are featured in Figure *s-s*. Both stress-strain curves show that the specimen increased in length at first, which is caused by the thermal expansion of the specimen during heating. After loading, the curve obtained at 1300 °C exhibits a flow-stress that remains fairly constant until a true strain of -0.7 is attained. As elaborated earlier, the temperature starts to decrease at this stage which, correspondingly, leads to a higher flow-stress. The discontinuity in the curve stems from the short period of time during which the deformation was paused. At 1220 °C, the flow-stress shows a peak and then gradually declines until a true strain of -0.77 is reached. At this point, similarly to the aforementioned experiment, the specimen temperature started to drop. For comparison, the results of compression experiments performed at a Gleeble thermo-mechanical simulator are shown in the inset. These experiments were conducted at a constant strain rate of 5×10^{-3} s^{-1} and temperatures of 1200 °C and 1300 °C.
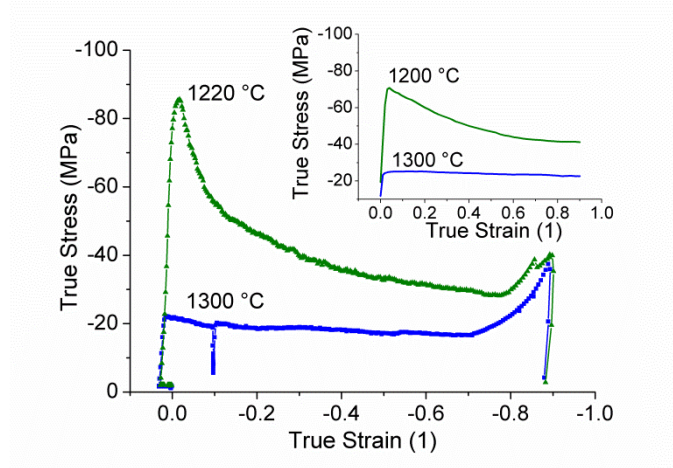
Figure *s-s*: Stress-strain curves of specimens deformed at 1300 °C (α+β phase field region) and 1220 °C (α+β+γ phase field region). The data were acquired during the in-situ experiment where the specimen was deformed at a mean strain rate of 3.7×10^{-3} 1/s. The inset shows the results of experiments conducted with a Gleeble thermo-mechanic simulator at temperatures of 1200 °C and 1300 °C at a strain rate of 5×10^{-3} s^{-1}.

After deformation, the specimens used in the in-situ experiments were investigated with regard to their microstructure by means of EBSD. Kernel average misorientation maps of the specimen deformed at 1300 °C are presented in Figure *EBSD1300*. In this mode, the misorientations between a center point and its next-nearest neighbors are evaluated. The average misorientation is then calculated and assigned to the center point. Details on this procedure can be found in [41,42]. A number of sub-grain boundaries are visible in the α_2-phase grains. Additionally, high degrees of misorientation are observed within some grains. In contrast to this, the β_o grains exhibit rather low defect densities.
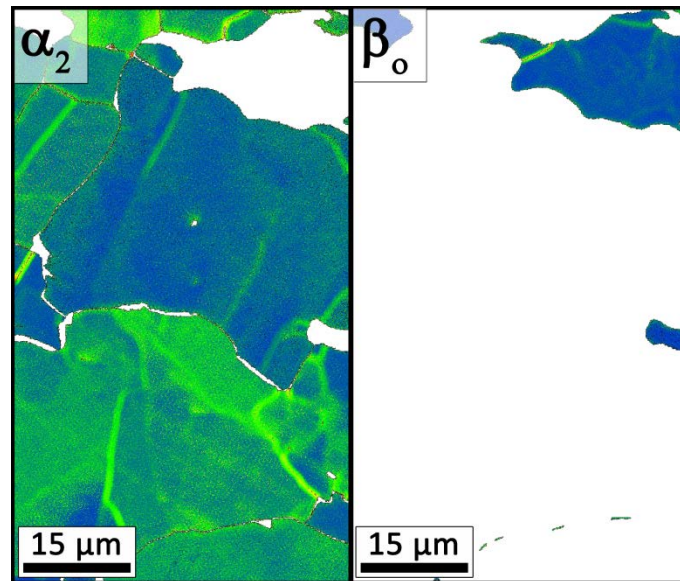
15

Figure *EBSD1300*: Kernel average misorientation maps of α_2 and β_o-phase obtained by EBSD (light colors correspond to high misorientations). The images show the microstructure of the specimen after deformation at 1300 °C. Note that both phases were disordered at 1300 °C.

In Figure *EBSD1220*, kernel average misorientation maps of the specimen deformed at 1220 °C is shown. At this temperature three phases (α, β and γ) were present during deformation. Due to the precipitation of fine γ-lamellae during cooling (after deformation), the α_2-phase was not properly resolved in the EBSD image. The γ-phase is only imaged if present in the form of globular grains or coarse lamellae. In these areas, some low-angle grain boundaries (LAGBs) and orientation gradients within grains are observed. It is obvious from Figure *EBSD1220* that, apart from a few LAGBs, only a low number of defects were stored in the β_o-phase. The misorientation plot of the γ-phase reveals the presence of sub-grain boundaries and of certain areas of high misorientation especially in coarse lamellae.
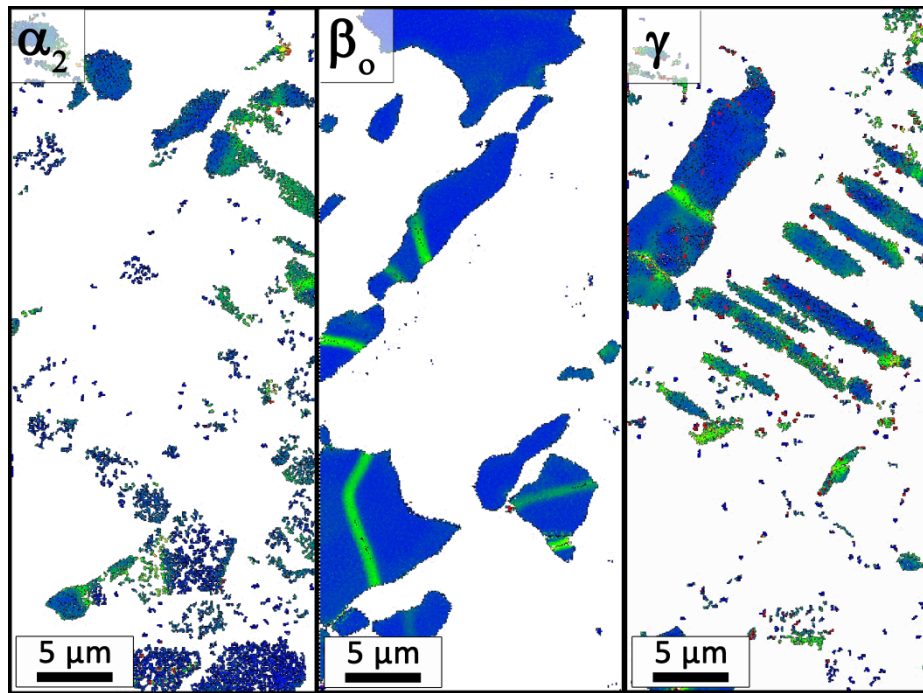
Figure *EBSD1220*: Kernel average misorientation maps obtained after deformation of the specimen at 1220 °C. Due to high defect densities within the γ and the α$_2$-phase and the lamellar arrangement of the two phases, only the β$_o$-grains are imaged properly. Light colors correspond to high degrees of misorientation. Note that at 1220 °C, α and β-phase present in their disordered state.

4 Discussion

The reason for implementing complex hot-deformation steps in the production route of TiAl parts is to improve the microstructure and therefore the mechanical properties of the product [1,2,4,7,43,44]. A comparison between the microstructures present before (Figure *cast*) and after (Figure *def*) hot-deformation shows that the grains elongated perpendicular to the compression direction during plastic deformation. After hot-compression at 1220 °C, many lamellar grains are oriented with the lamellae perpendicular to the load axis (Figure *def*b). This observation is explained by the fact that lamellar colonies exhibit a deformation behavior that is similar to a stack of cards. If the lamellae are perpendicular to the loading direction,

the colony is in hard mode because the α-phase (or below the ordering temperature α$_2$-phase) has to deform in its hardest slip mode. In the soft mode, the lamellae enclose an intermediate angle (ideally 45°) with respect to the loading direction and deform easily via shear parallel to the interfacial planes. Colonies in which the lamellae are parallel to the load exhibit an intermediate yield stress [45].

The elongated shape of the β$_o$-grains after deformation suggests that disordered β accommodated a disproportionally large fraction of the strain (Figure *def*). This finding is in accord with literature results [46]. Additionally, it is commonly known that hot-deformation at lower temperatures leads to finer grained microstructures [47] which is confirmed by Figures *def*a and *def*b and previous studies conducted on various TiAl alloys, e.g. [46,48,49].

4.1 α-phase

The results from in-situ HEXRD experiments allow bridging the gap between the microstructural images before and after the compression experiment. In the AT-plots of both investigated deformation temperatures, the α timelines tilt and broaden as soon as deformation starts (Figures *AT*a and d). This indicates the occurrence of grain rotation about the beam axis and defect formation (i.e. dislocation multiplication). Timelines frequently bifurcate at 1300 °C, which is less frequently observed at 1220 °C. Bifurcation can be caused by the arrangement of dislocations to sub-grain boundaries which infers that at 1220 °C processes that lead to such an arrangement occur less readily. Another notable difference is that timelines remain sharper during deformation at 1300 °C, than at 1220 °C (Figures *AT* a and d).

Sharp timelines or dots appear in significant numbers at a strain of ~0.25 (at t=250 s) while the material is being deformed at 1220 °C. This infers that new grains with low defect density appear after some minimum plastic strain and time. Dynamic

discontinuous recrystallization (DDRX) is known to require a minimum amount of plastic deformation and a so-called incubation time [50]. Consequently, the observation of the sudden appearance of grains with low defect density can be ascribed to DDRX.

At 1300 °C, the dominant features in the AT-plot of the α 022 reflection are long timelines that show moderate broadening (Figure *AT* a). Instantaneous bifurcation of timelines upon the onset of compression points towards the accommodation of defects by a continuous process that does neither require a minimum strain, nor an incubation time. An important factor in determining which process is likely to contribute most to accommodating the defects is the SFE. No accurate values of the stacking fault energy (SFE) in the α/α$_2$-phase are to be found in literature, but there seems to be some consensus on the fact that it is high [46] which favors dynamic recovery (DRV). Considering these facts it is concluded that the α-phase undergoes a significant degree of recovery at 1300 °C. Additionally, HAGB formation may occur by continuous recrystallization. In general, the defect densities in the α-phase are high after deformation which is in accord with the findings of Liu et al. [46].

The EBSD map of the α$_2$-phase after deformation at 1300 °C (Figure *EBSD1300*) reveals that grains with different defect densities are present. Additionally, sub-grain boundaries are observed in the microstructure which confirms the occurrence of DRV.

4.2 β-phase

Contrary to the AT-plots of the α-phase, those of the β-phase show strong similarities at the two investigated temperatures (Figure *AT* b and e). In both experiments, changes in the timelines of the β-phase are obvious even before

deformation starts at t~125 s. Since no strain is imposed on the specimen at this stage, only grain coarsening and phase transformation processes can change the intensity of a diffraction spot. Although there are single timelines vanishing and appearing during this stage, continuous timelines are far more dominant. This suggests that only a few grains are affected by the aforementioned processes. As soon as the specimen is subjected to deformation, the timelines disintegrate into clouds of small, comparatively sharp reflection spots located around the position of the original timeline. Many sharp spots with low intensities within a small angular range correspond to a large number of rather small crystallites with low defect densities and small misorientations [35]. Consequently, it is concluded that DRV is the dominant process. This conclusion is supported by the fact that the bcc β-phase is presumed to have a high SFE due to its similarity to β-Ti [46,51]. Additionally, it has been found for a different TiAl alloy [46] that the β-phase accommodates a large fraction of plastic strain during hot-deformation, which is confirmed by the morphology of the β-phase shown in Figure *def*.

The main difference between the AT-plots obtained at the two different temperatures is that the reflection spots are sharper and of higher intensity at 1300 °C compared to 1220 °C (Figures *AT* b and e). This behavior is attributed to the fact that thermally activated recovery processes are occurring faster at higher temperatures.

Since both experiments were performed at the same strain rate, more rapidly occurring DRV processes lead to lower defect densities in steady-state conditions. Furthermore, the flow-stress has a pronounced influence on the sub-cell size [52,53]. The lower the flow-stress, the larger the sub-cells, which explains the higher intensity of reflection spots at 1300°C. From EBSD results (Figure *EBSD1220*), it is obvious

that the β_o-phase grains have low defect densities. Some sub-grain boundaries are observed, especially after deformation at 1220 °C, confirming the occurrence of DRV.

4.3 γ-phase

Deformation at 1220°C is performed in the (α+β+γ) phase field region. During heating, the volume fraction of γ-phase is decreasing (Figure *phase* b) which is reflected by the overall loss in intensity visible in the AT-plot (Figure *ATg* a). One important fact to notice is that the γ-phase is present in the form of globular grains and as lamellae within the α/γ lamellar colonies at deformation temperature. Since γ and α laths of the same colony are in the Blackburn orientation relationship [54], a colony images similarly to globular γ-grains in the AT-plot. The fluctuations in intensity before deformation starts (Figure *ATg* a) are attributed to coarsening and phase transformation processes. As a plastic strain is imposed on the specimen, most timelines broaden and tilt. However, there are some timelines that tilt but do not broaden significantly. These timelines are believed to origin from lamellar colonies that occupy a hard orientation with respect to the compression axis. Consequently, these grains accommodate a smaller fraction of the total strain and therefore show a lower defect density than the ones occupying a soft orientation. Rotation of these grains is facilitated by the plastic deformation of grains that surround them and are deformed more readily. Coarse lamellar colonies in hard orientations are likely to persist in the deformed microstructure, since the strains imposed are too small to induce recrystallization in the γ-phase. Most lamellar colonies in soft orientation, however, recrystallize more readily because of their higher defect density. It should be noted, at this point, that the strain imposed on a lamellar colony is not only dependent on its orientation, but also critically on its surrounding microstructural components.

From the experimental observations, e.g. see Figure *def* b it is concluded, that a significant fraction of the γ-phase undergoes DDRX during hot working at 1220 °C. Dynamic recovery occurs less readily due to the small SFE of γ (60-90 mJ/m^2 [46]). Chraponski et al. [55] investigated a γ-TiAl based alloy which was hot-worked at 1000 °C by means of transmission electron microscopy and concluded that recrystallization as well as recovery occur in the γ-phase which is in excellent agreement with the present study. Additionally, this publication [55] points out that there is a significant degree of deformation inhomogeneity which is also confirmed by the current results.

4.4 Flow-curve

Generally, the shape of the flow-curve can be used to determine the restoration mechanisms that are operative during hot-deformation. Flow-curves recorded during the experiment are similar to those obtained with a Gleeble thermo-mechanical simulator (Figure *s-s*). A common interpretation of flow-curves is based on their shape. Single-peak flow curves are indicative of dynamic recrystallization, whereas a constant flow stress is associated with the occurrence of dynamic recovery (e.g. [47]). The flow curve obtained from the experiment performed at 1300 °C exhibits an approximately constant stress level until the temperature drops (Figure *s-s*). This indicates that dynamic recovery processes are dominant, whereas the flow curve obtained at 1220 °C corresponds to the single-peak type indicating softening due to dynamic recrystallization. At 1300 °C, the HEXRD data show clear evidence that dynamic recovery occurs in both, α and β-phase which is in excellent accord with the observed shape of the flow-curve (Figure *s-s*). Deformation at 1220 °C leads to a flow curve that exhibits significant flow-softening. By HEXRD, it was found that a large fraction of the lamellar colonies decomposes

and that the γ-phase recrystallizes dynamically. Furthermore, α-grains were shown to recrystallize at this temperature. Since only small fractions of β are present at this temperature (see Figure *phase* b), the shape of the flow curve is consistent with the findings of the HEXRD experiment.

Conclusion

In this paper, the hot-deformation behavior of a Ti-43.5 Al-4 Nb-1 Mo-0.1 B alloy was investigated in-situ by means of high-energy X-ray diffraction. The compression experiments were conducted at 1300 °C in the (α+β) phase field region and at 1220 °C in the (α+β+γ) phase field region at a mean strain rate of 0.0037 s^{-1}. It was found that the α-phase predominantly dynamically recovers at 1300 °C, whereas dynamic recrystallization is observed for strains exceeding 0.25 at 1220 °C. For the β-phase, dynamic recovery was determined as dominant process at both temperatures. The γ-phase dynamically recovers and recrystallizes at 1220 °C. By means of in-situ HEXRD, it was also possible to directly observe the behavior of lamellar colonies which initially occupied a hard orientation with respect to the compression axis. Even though some of these colonies rotated during compression, they accommodated hardly any strain. Consequently, the defect density was too low to induce dynamic recrystallization and remnant colonies were found during post-mortem microstructural examinations. Results obtained by complementary investigation methods are in good agreement with the behavior observed in the HEXRD experiments. In this study, in-situ methods were used to gain insight into the microstructural evolution during hot-working of a β-containing γ-TiAl based alloy. The obtained results yield important information for future alloy design strategies and for the optimization of industrial-scale hot-deformation processes of β containing γ-TiAl alloys.

References

[1]   Kim Y-W, Clemens H, Rosenberger A, editors. Gamma Titanium Aluminides 2003. Warrendale, PA, USA: TMS (The Minerals, Metals & Materials Society), 2003.

[2]   Yamaguchi M, Inui H, Ito K. Acta materialia 2000;48:307-322.

[3]   Appel F, Wagner R. Materials science and engineering: r: reports 1998;22:187-268.

[4]   Kestler H, Clemens H. Production, processing and application of γ(tial)-based alloys. In: Leyens C, Peters M, editors. Titanium and Titanium Alloys. Weinheim, Germany: WILEY-VCH, 2003. p. 351.

[5]   Wu X. Intermetallics 2006;14:1114-1122.

[6]   Cui W, Liu C, Bauer V, Christ H. Intermetallics 2007;15:675-678.

[7]   Clemens H, Smarsly W. Advanced materials research 2011;278:551-556.

[8]   Lasalmonie A. Intermetallics 2006;14:1123-1129.

[9]   Loria E. Intermetallics 2000;8:1339-1345.

[10]   Clemens H, Wallgram W, Kremmer S, Güther V, Otto A, Bartels A. Advanced engineering materials 2008;10:707-713.

[11]   Clemens H, Chladil HF, Wallgram W, Zickler GA, Gerling R, Liss K-D, Kremmer S, Guther V, Smarsly W. Intermetallics 2008;16:827-833.

[12] Kremmer S, Chladil H, Clemens H, Otto A, Güther V. Near conventional forging of titanium aluminides. In: Niinomi M, Akiyama S, Ikeda M, Hagiwari M, Maruyama K, editors. Ti-2007 Science and Technology. Sendai, Japan: The Japan Institute of Metals (JIM), 2008. pp. 989-992.

[13] Wallgram W, Schmoelzer T, Cha L, Das G, Güther V, Clemens H. International journal of materials research (formerly zeitschrift fuer metallkunde) 2009;100:1021-1030.

[14] Rizzi N. n.d.

[15] Shi JD, Pu Z, Zhong Z, Zou D. Scripta metallurgica et materialia 1992;27:1331-1336.

[16] Tetsui T, Shindo K, Kaji S, Kobayashi S, Takeyama M. Intermetallics 2005;13:971-978.

[17] Tetsui T, Shindo K, Kobayashi S, Takeyama M. Intermetallics 2003;11:299-306.

[18] Tetsui T, Shindo K, Kobayashi S, Takeyama M. Scripta materialia 2002;47:399-403.

[19] Appel F, Oehring M, Paul JDH, Klinkenberg C, Carneiro T. Intermetallics 2004;12:791-802.

[20] Liu B, Liu Y, Zhang W, Huang JS. Intermetallics 2011;19:154-159.

[21] Niu HZ, Chen YY, Xiao SL, Kong FT, Zhang CJ. Intermetallics 2011;19:1767-1774.

[22] Rao KP, Prasad YVRK, Suresh K. Materials & design 2011;32:4874-4881.

[23] Rao KP, Prasad YVRK. Materials science and engineering: a 2010;527:6589-6595.

[24] Wang G, Xu L, Tian Y, Zheng Z, Cui Y, Yang R. Materials science and engineering: a 2011;528:6754-6763.

[25] Witusiewicz VT, Bondar A, Hecht U, Rex S, Velikanova T. Journal of alloys and compounds 2008;465:64-77.

[26] Clemens H, Boeck B, Wallgram W, Schmoelzer T, Droessler LM, Zickler GA, Leitner H, Otto A. Experimental studies and thermodynamic simulations of phase transformations in ti-(41-45)al-4nb-1mo-0.1b alloys. In: MRS Proceedings, vol. 1128. Warrendale: MRS, 2008. pp. 115-120.

[27] Schmoelzer T, Liss K-D, Zickler GA, Watson IJ, Droessler LM, Wallgram W, Buslaps T, Studer AJ, Clemens H. Intermetallics 2010;18:1544-1552.

[28] Schloffer M, Iqbal F, Gabrisch H, Schwaighofer E, Schimansky F-P, Mayer S, Stark A, Lippmann T, Göken M, Pyczak F, Clemens H. Intermetallics 2012;22:231-240.

[29] Liss K-D, Garbe U, Li H, Schambron T, Almer JD, Yan K. Advanced engineering materials 2009;11:637–640.

[30] Liss K-D, Yan K. Materials science and engineering: a 2010;528:11-27.

[31] Liss K-D, Schmoelzer T, Yan K, Reid M, Dippenaar R, Clemens H. Journal of applied physics 2009;106:113526.

[32] Saunders N. Gamma titanium aluminides, the minerals, metals & materials society (tms), warrendale, pa 1999:183–194.

[33] Watson IJ, Liss K-D, Clemens H, Wallgram W, Schmoelzer T, Hansen TC, Reid M. Advanced engineering materials 2009;11:932-937.

[34] Daniels JE, Drakopoulos M. Journal of synchrotron radiation 2009;16:463–468.

[35] Jakobsen B, Poulsen H, Lienert U, Almer JD, Shastri SD, Sørensen HO, Gundlach C, Pantleon W. Science (new york, n.y.) 2006;312:889-92.

[36] Warren BE. X-ray Diffraction. New York: Dover Publications, 1990.

[37] Margulies L, Winther G, Poulsen H. Science 2001;291:2392.

[38] Yan K, Liss K-D, Garbe U, Daniels JE, Kirstein O, Li H, Dippenaar R. Advanced engineering materials 2009;11:771-773.

[39] Schmoelzer T, Liss K-D, Staron P, Mayer S, Clemens H. Advanced engineering materials 2011;13:685-699.

[40] Reimers W, Pyzalla AR, Schreyer A. Neutrons and Synchrotron Radiation in Engineering Materials Science. Weinheim, Germany: WILEY-VCH, 2008.

[41] Rehrl C, Kleber S, Renk O, Pippan R. Materials science and engineering: a 2011;528:6163-6172.

[42] Vorhauer A, Hebesberger T, Pippan R. Acta materialia 2003;51:677-686.

[43] Kim Y-W, Morris D, Yang R, Leyens C, editors. Structural Aluminides for Elevated Temperature Applications. Warrendale, PA, USA: TMS (The Minerals, Metals & Materials Society), 2008.

[44] Kim Y-W. Acta metallurgica et materialia 1992;40:1121–1134.

[45] Inui H, Kishida K, Misaki M, Kobayashi M, Shirai Y, Yamaguchi M. Philosophical magazine a 1995;72:1609-1631.

[46] Liu B, Liu Y, Li YP, Zhang W, Chiba A. Intermetallics 2011;19:1184-1190.

[47]   Dieter GE. Mechanical Metallurgy. Boston: Mcgraw Hill Higher Education, 1989.

[48]   Appel F, Kestler H, Clemens H. Forming. In: Wesstbrook JH, Fleischer RL, editors. Intermetallic Compounds - Principles and Practice: Progress. Chichester, UK: John Wiley & Sons Ltd., 2002. pp. 617-642.

[49]   Seetharaman V, Semiatin SL. Metallurgical and materials transactions a 1996;27:1987-2004.

[50]   Humphreys FJ, Hatherly M. Recrystallization and Related Annealing Phenomena. Pergamon Press Ltd., 2004.

[51]   Leyens C, Peters M, editors. Titanium and Titanium Alloys. Weinheim, Germany: Wiley-VCH, 2003.

[52]   Raj S, Pharr GM. Materials science and engineering 1986;81:217-237.

[53]   Orlová A. Materials science and engineering a 1996;220:281-285.

[54]   Blackburn MJ. No title. In: Jaffee RI, Promisel NE, editors. The Science, Technology and Application of Titanium. Oxford: Pergamon Press Ltd., 1970. p. 663.

[55]   Chrapoński J, Rodak K. Journal of microscopy 2006;223:298-301.